The International Journal of Cardiovascular Imaging (2019) 35:1119–1132
https://doi.org/10.1007/s10554-019-01544-6

ORIGINAL PAPER

Impact of age and cardiac disease on regional left and right ventricular myocardial motion in healthy controls and patients with repaired tetralogy of fallot

Alexander Ruh[1] · Roberto Sarnari[1] · Haben Berhane[2] · Kenny Sidoryk[1] · Kai Lin[1] · Ryan Dolan[1] · Arleen Li[3] · Michael J. Rose[2] · Joshua D. Robinson[1,4,5] · James C. Carr[1] · Cynthia K. Rigsby[1,2,5] · Michael Markl[1,6]

Received: 7 December 2018 / Accepted: 21 January 2019 / Published online: 4 February 2019

Abstract

The assessment of both left (LV) and right ventricular (RV) motion is important to understand the impact of heart disease on cardiac function. The MRI technique of tissue phase mapping (TPM) allows for the quantification of regional biventricular three-directional myocardial velocities. The goal of this study was to establish normal LV and RV velocity parameters across a wide range of pediatric to adult ages and to investigate the feasibility of TPM for detecting impaired regional biventricular function in patients with repaired tetralogy of Fallot (TOF). Thirty-six healthy controls (age = 1–75 years) and 12 TOF patients (age = 5–23 years) underwent cardiac MRI including TPM in short-axis locations (base, mid, apex). For ten adults, a second TPM scan was used to assess test–retest reproducibility. Data analysis included the calculation of biventricular radial, circumferential, and long-axis velocity components, quantification of systolic and diastolic peak velocities in an extended 16 + 10 LV + RV segment model, and assessment of inter-ventricular dyssynchrony. Biventricular velocities showed good test–retest reproducibility (mean bias ≤ 0.23 cm/s). Diastolic radial and long-axis peak velocities for LV and RV were significantly reduced in adults compared to children (19–61%, $p < 0.001$–0.02). In TOF patients, TPM identified significantly reduced systolic and diastolic LV and RV long-axis peak velocities (20–50%, $p < 0.001$–0.05) compared to age-matched controls. In conclusion, tissue phase mapping enables comprehensive analysis of global and regional biventricular myocardial motion. Changes in myocardial velocities associated with age underline the importance of age-matched controls. This pilot study in TOF patients shows the feasibility to detect regionally abnormal LV and RV motion.

Keywords Cardiovascular magnetic resonance · Tissue phase mapping · Biventricular myocardial velocities · Inter-ventricular dyssynchrony · Repaired tetralogy of Fallot · Children

✉ Alexander Ruh
alexander.ruh@northwestern.edu

1 Department of Radiology, Feinberg School of Medicine, Northwestern University, 737 N. Michigan Avenue, Suite 1600, Chicago, IL 60611, USA

2 Department of Medical Imaging, Ann & Robert H. Lurie Children's Hospital of Chicago, Chicago, IL, USA

3 Feinberg School of Medicine, Northwestern University, Chicago, IL, USA

4 Division of Pediatric Cardiology, Department of Pediatrics, Ann & Robert H. Lurie Children's Hospital of Chicago, Chicago, IL, USA

5 Department of Pediatrics, Feinberg School of Medicine, Northwestern University, Chicago, IL, USA

6 Department of Biomedical Engineering, McCormick School of Engineering, Northwestern University, Evanston, IL, USA

Introduction

Assessment of both left (LV) and right ventricular (RV) function is important for prognosis in congenital heart disease [1]. While assessing RV function by echocardiography remains challenging [2], cardiovascular MRI has emerged as a robust and reproducible imaging technique to obtain global functional parameters such as RV ejection fraction [3, 4]. In addition, MRI techniques such as MR tagging, displacement encoding with stimulated echoes (DENSE), or 2D cine phase contrast MRI have been employed to assess regional RV function [5–8], enabling biventricular functional analysis to characterize changes in ventricular interactions in different cardiac pathologies [8–10].

Tetralogy of Fallot (TOF) is the most common cyanotic congenital heart disease [11], which is usually surgically

repaired during the first year of life with a survival rate of more than 98% [12]. However, residual anatomical and functional abnormalities are common and require lifelong surveillance and possibly further treatment [13–16]. However, standard cardiac MRI assessments [16] based on global parameters [17–19] may not reflect regional myocardial abnormalities or ventricular interactions. More recently, MR tagging [10, 20] and MR feature tracking [8, 9, 21–23] studies evaluating regional motion and biventricular interaction have been performed that showed reduced biventricular strain [8, 9, 20] as well as increased inter-ventricular dyssynchrony [10, 21].

In this context, 2D cine phase contrast MRI with three-directional velocity encoding, termed tissue phase mapping (TPM), is a well-established technique to quantify LV regional myocardial velocities [24–41] but has rarely been applied to the RV. In 2000, Kayser et al. [6] analyzed RV wall motion with TPM for the first time, and more recently biventricular function in healthy adults [42] and adult patients with pulmonary hypertension [43] have been investigated. However, current studies lack a systematic assessment of (1) test–retest reproducibility of biventricular TPM, (2) normal LV and RV myocardial velocities across a wide range of pediatric to adult ages, and (3) the sensitivity of TPM to detect differences in regional biventricular function in patients with repaired TOF.

It was the purpose of this study to apply a biventricular TPM analysis workflow for the comprehensive quantification of regional LV and RV velocities (mapped to an extended 16 + 10 LV + RV segment model), LV and RV velocity twist, as well as inter-ventricular dyssynchrony. In addition, TPM was used to assess cardiac function in a cohort of patients with repaired TOF to test the hypothesis that TPM can identify regional functional abnormalities involving both LV and RV.

Materials and methods

Study population

The study population included 36 healthy controls (age = 32 ± 20 years, 21 male) spanning a large age range from 1 to 75 years. For further analysis, the control cohort was subdivided in an adult (n = 18, age = 49 ± 15 years, 12 male) and pediatric group (n = 18, age = 15 ± 4 years, nine male). In addition, 12 patients with repaired TOF (age = 15 ± 5 years, six male) were included.

Adult healthy subjects were recruited for a research MRI based on an IRB-approved protocol and after providing written informed consent. Healthy children and TOF patients underwent a physician-ordered cardiac MR assessment. After written informed consent was obtained, TPM was performed as part of this IRB-approved and HIPAA-compliant study. Healthy children underwent cardiac MRI for evaluation of structural or ischemic heart disease due to syncope, chest pain, palpitations, or family history of arrhythmogenic right ventricular cardiomyopathy, but these initial diagnoses were ruled out by negative MRI studies and negative clinical work up. Two healthy children and four TOF patients were under general anesthesia during the scan, which is standard for pediatric patients who cannot remain still either due to young age or developmental delay.

All TOF patients were imaged following complete surgical repair (14 ± 5 years post-surgery at time of MRI) using a pulmonary valve-sparing procedure in one patient and a transannular patch in 11 patients. Of the latter, three patients subsequently underwent pulmonary valve replacement, and one patient with additional pulmonary atresia, who received a pericardial monocusp during complete repair, eventually needed a pulmonary homograft.

MRI data acquisition

All subjects underwent cardiac MRI at 1.5T (MAGNETOM Aera, Siemens, Erlangen, Germany) including k–t accelerated TPM using a prospectively ECG-gated, black-blood prepared gradient echo sequence with three-directional velocity encoding [24, 25, 30]. Time-resolved TPM images were acquired for about 80% of the cardiac cycle (omitting late diastole due to prospective ECG triggering) for three short-axis slices at basal, mid-ventricular and apical locations as illustrated in Fig. 1a. Spatiotemporal imaging acceleration using PEAK-GRAPPA [44, 45] with an undersampling factor of R = 5 (ten reference lines, net acceleration factor R_{net} = 3.0–4.1) permitted data acquisition during breath-holding (breath-hold time = 20–30 heart beats per slice except for one TOF patient under general anesthesia with 46 heart beats per slice). Additional imaging parameters were as follows: echo time = 3.4–3.8 ms; repetition time (TR) = 5.1–6.3 ms; temporal resolution = 4 · TR = 20.4–25.2 ms; flip angle = 10°/15°; bandwidth = 455–655 Hz/pixel; velocity encoding = 25 cm/s in all directions; matrix size = 160–256 × 60–190; interpolated in-plane resolution = $(1.3–1.9\ mm)^2$ for children aged 1–10 years, $(1.8–2.1\ mm)^2$ for children aged 11–14 years, $(1.8–2.4\ mm)^2$ for adolescents aged 15–19, and $(1.8–2.3\ mm)^2$ for adults aged 20 years and older; slice thickness = 5–8 mm. Image reconstruction on the MR scanner yielded magnitude images as well as in-plane (v_x and v_y) and through-plane (v_z) velocity images for all time frames and slices. For ten adults a second TPM scan, performed 15 ± 5 days after the first, was analyzed to test the reproducibility of the biventricular velocity assessment. Global cardiac function parameters for all subjects were obtained from

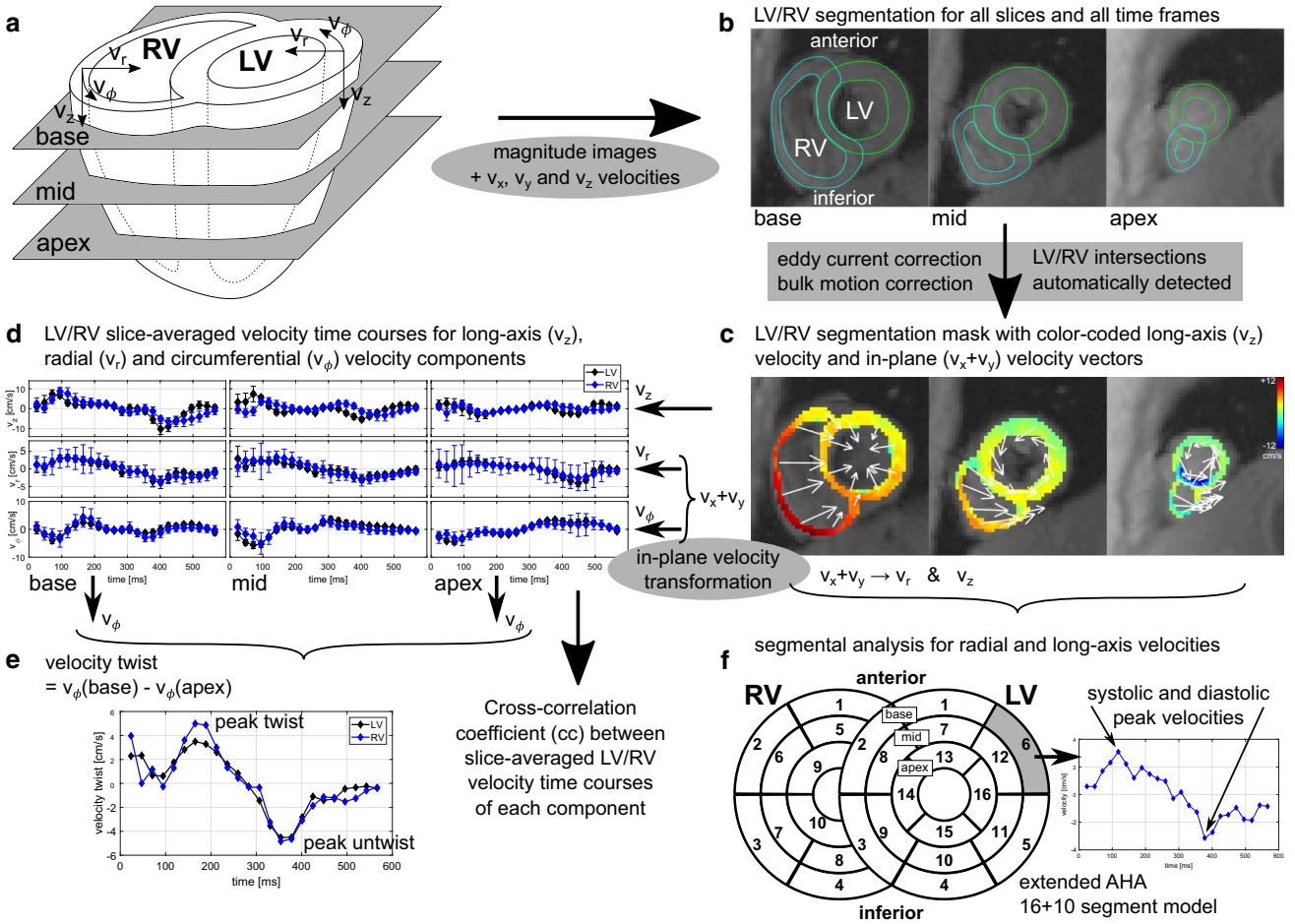

Fig. 1 Schematic depiction of the workflow for biventricular TPM analysis. **a** Magnitude and three-directional velocity images (v_x, v_y, v_z) were acquired for three short-axis slices (base, mid, apex). **b** LV/RV epi- and endocardial borders were contoured to obtain myocardial masks. The LV/RV intersection points were automatically detected, and the septum was excluded from the RV mask. **c** After eddy current and in-plane bulk motion corrections, the three-directional velocity information can be visualized by color-coding in through-plane direction and in-plane velocity vectors. **d** For both ventricles, the Cartesian in-plane velocities (v_x, v_y) were transformed into radial (v_r) and circumferential (v_ϕ) components. Slice-averaged velocity time courses were obtained for LV and RV. **e** Velocity twist was calculated as the difference between circumferential velocity time courses at base and apex, and peak systolic twist and peak diastolic untwist were extracted. To investigate inter-ventricular dyssynchrony, cross-correlation coefficients between LV/RV velocity time courses were calculated for v_r, v_ϕ, and v_z. **f** Based on an extended 16 + 10 AHA model, biventricular regional systolic and diastolic radial and long-axis peak velocities were calculated for each segment

standard, retrospectively ECG-gated short-axis cine steady state free precession images.

Biventricular TPM data analysis

Post-processing and data analysis were performed using a custom software package developed in MATLAB (MathWorks, Natick, MA, USA). The data analysis workflow is schematically depicted in Fig. 1. First, the magnitude data in short-axis view was used to segment the epi- and endocardial LV and RV borders for all three slices and cardiac time frames. In a semi-automatic procedure, manually set nodes were interpolated by splines to obtain smooth segmentation contours (Fig. 1b), which enclose LV and RV myocardial masks. The anterior and inferior intersections of the two ventricles were automatically detected for all time frames and used to remove the septum from the RV masks. For segmental analysis the American Heart Association (AHA) 16-segment model [46] was used, which was expanded by a 10-segment RV extension, Fig. 1f [42]. The RV free wall segments were defined to have equal angles between the LV/RV intersection points. If the basal slice included the transition between the LV/RV outflow tracts and the aorta/pulmonary artery instead of the septal LV or anterior RV wall, respectively, affected segments were manually excluded from the LV/RV mask and further analysis to avoid artefacts from blood velocities. End-systole was detected automatically as the time

frame with the smallest endocardial LV volume (summed over all three slices).

All TPM velocity data were 3 × 3 median filtered and subsequently corrected for eddy currents by subtracting an offset plane, which was fitted to the static tissue [47]. To remove in-plane bulk motion from the velocity fields, a correction similar to Ref. [24], which is based on subtraction of global LV translation velocities from the pixelwise velocities, was performed. To better resemble contraction and rotation of the ventricles, the Cartesian in-plane velocities within the LV and RV masks (v_x, v_y) were transformed to radial and circumferential components (Fig. 1a), which were defined to be orthogonal (v_r) and tangential (v_ϕ) to the local segmentation contours. For each myocardial pixel the normal vectors to both epi and endocardial contours were calculated, and the final radial direction was set to the mean of those two vectors. Positive velocities represent radial contraction, clockwise rotation (as seen from the apex), and shortening in long-axis direction (v_z) as defined in Fig. 1a. For each velocity component, pixelwise velocities from the LV and RV segmentation masks were averaged within slices (base, mid, apex) and individual segments (16 + 10 LV + RV) to obtain LV and RV velocity time courses for all slices and segments. To correct for residual bulk motion all velocity time courses were shifted to a zero temporal mean.

For radial and long-axis velocity components, systolic and diastolic peak velocities were extracted from the velocity time courses in the biventricular 16 + 10 segment model, Fig. 1f [26]. Subsequently, global LV and RV peak velocities were obtained by averaging the segmental values for each ventricle. To quantify circumferential motion of the ventricles, velocity twist was calculated as the difference between circumferential velocity time courses from base and apex, and values for peak systolic twist and peak diastolic untwist were obtained, Fig. 1d, e [27]. Finally, to assess the synchrony/dyssynchrony between LV and RV function, the cross-correlation coefficient (cc) between the slice-averaged LV and RV velocity time courses (Fig. 1d) was calculated. The data for all three slices was combined to obtain a single coefficient for each velocity component. The resulting cc coefficient is a measure of inter-ventricular dyssynchrony (cc = 1: completely synchronous LV and RV motion, reduced cc = increased dyssynchrony).

Statistical analysis

All continuous data are presented as mean ± standard deviation. To assess differences between cohorts, TPM data in children were compared to adults on the global and segmental (16 + 10 LV + RV AHA model) level. To investigate changes in myocardial velocities in TOF patients, an age-matched healthy control cohort of 19 subjects was used (17 children and two adults, nine male, age = 17 ± 3 years, $p = 0.2$). All data were first tested for normality with a Lilliefors test followed by unpaired t-tests for normally distributed data or Wilcoxon rank-sum tests for non-normally distributed data to identify significant differences between groups. The reproducibility of biventricular TPM analysis was assessed by a Bland–Altman comparison of segmental peak velocities and peak twist values for both ventricles in systole and diastole obtained from two independent scans. Additionally, global test–retest velocities were compared using paired t-tests and Wilcoxon signed-rank tests, depending on the results of Lilliefors tests. For the total cohort of healthy subjects linear regression was performed, and Pearson's correlation coefficient r was calculated to identify relationships between global peak velocities and body surface area (BSA). For this, absolute velocities were used so that positive correlations are always associated with increased velocities independent of sign. Results were considered significant for $p < 0.05$.

Results

Global LV and RV function

Demographic data for all study cohorts are summarized in Table 1. For both LV and RV, end-diastolic volume index (EDVI, $p < 0.001$), end-systolic volume index (ESVI, $p < 0.001$), and stroke volume index (SVI, $p < 0.02$) were significantly reduced in adults compared to children. On the other hand, LV ejection fraction (EF) was higher in adults compared to children ($p = 0.005$). Compared to the control cohort, TOF patients showed reduced LV ($p = 0.02$) and RV ($p < 0.001$) EF and increased RV EDVI ($p < 0.001$), ESVI ($p < 0.001$), and SVI ($p = 0.015$).

Biventricular TPM test–retest reproducibility

Bland–Altman plots for the test–retest analysis conducted in ten adults are depicted in Fig. 2. Segmental radial and long-axis peak velocities as well as global peak twist showed minimal mean differences (systole/diastole: −0.23/0.21 cm/s, 0.21/0.12 cm/s and −0.04/−0.13 cm/s, respectively) and moderate limits of agreement for systole and diastole with similar distributions of LV and RV values. Table 2 summarizes global LV and RV peak velocities and twist showing excellent agreement with no significant differences between the two scans ($p \geq 0.2$).

Regional biventricular motion patterns

Figure 3 shows biventricular myocardial velocities in a basal short-axis slice for representative subjects (57-year-old adult, 15-year-old child, 14-year-old TOF patient). Averaged

Table 1 Demographic data and global function parameters for healthy children and adults as well as TOF patients and age-matched controls

	Children	Adults	p-value	Controls	TOF patients	p-value
Male/female	9/9	12/6	0.5*	9/10	6/6	1.0*
Age (range) [years]	15 ± 4 (1–19)	49 ± 15 (20–75)	< 0.001	17 ± 3 (10–22)	15 ± 5 (5–23)	0.2
BSA (m^2)	1.6 ± 0.4	2.0 ± 0.3	< 0.001	1.6 ± 0.2	1.5 ± 0.3	0.15
Heart rate (bpm)	77 ± 15	68 ± 15	0.09	77 ± 15	74 ± 12	0.6
LV						
EDVI (ml/m^2)	**87 ± 14**	**69 ± 11**	**< 0.001**	87 ± 14	86 ± 11	0.9
ESVI (ml/m^2)	**37 ± 6**	**26 ± 6**	**< 0.001**	37 ± 6	44 ± 15	0.07
SVI (ml/m^2)	**50 ± 9**	**43 ± 7**	**0.013**	50 ± 9	46 ± 8	0.14
EF (%)	**58 ± 3**	**62 ± 5**	**0.005**	**58 ± 4**	**53 ± 8**	**0.02**
EDMI (g/m^2)	44 ± 10	52 ± 17	0.12	43 ± 10	43 ± 8	0.8
RV						
EDVI (ml/m^2)	**85 ± 16**	**65 ± 12**	**< 0.001**	**85 ± 16**	**126 ± 15**	**< 0.001**
ESVI (ml/m^2)	**38 ± 9**	**29 ± 6**	**< 0.001**	**38 ± 9**	**70 ± 14**	**< 0.001**
SVI (ml/m^2)	**48 ± 9**	**36 ± 7**	**< 0.001**	**47 ± 10**	**56 ± 10**	**0.015**
EF (%)	56 ± 5	56 ± 4	0.8	**55 ± 5**	**45 ± 7**	**< 0.001**

Bold face marks significant differences in global function ($p < 0.05$)

BSA body surface area calculated with the Mosteller formula, *EDVI* end-diastolic volume index, *ESVI* end-systolic volume index, *SVI* stroke volume index, *EF* ejection fraction, *EDMI* end-diastolic mass index

*Using Fisher's exact test

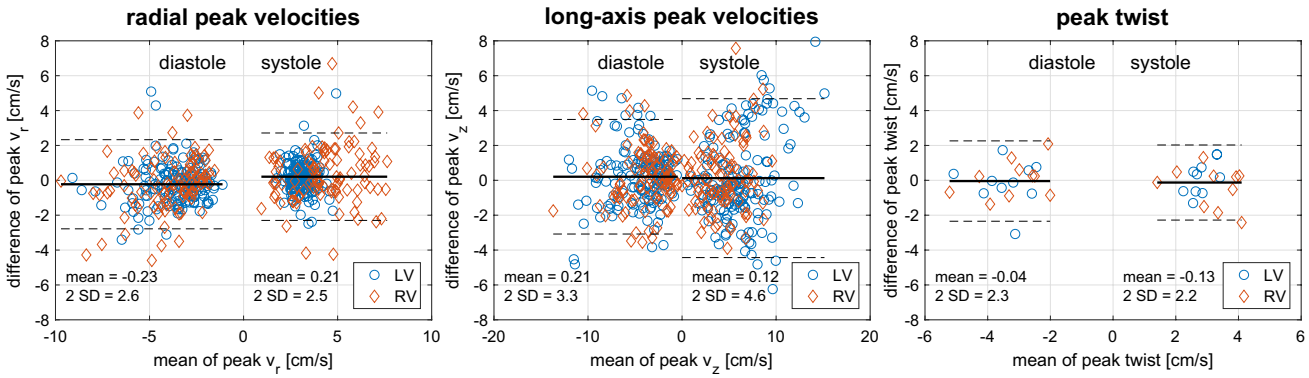

Fig. 2 Test–retest analysis for segmental peak velocities (16 LV and 10 RV segments) and global peak twist in ten adults for systole and diastole. Thick lines highlight the mean difference between the two scans and dashed lines show limits of agreement [±2 standard deviations (SD)]

velocity time courses (Fig. 3 top) depict the temporal evolution of long-axis (v_z), radial (v_r) and circumferential (v_ϕ) velocities over the cardiac cycle for LV (black lines) and RV (blue lines). Peak systolic and diastolic regional myocardial motion patterns are depicted in Fig. 3 bottom [color coding: through-plane long-axis (v_z) motion; arrows: regionally averaged in-plane velocity vectors].

Velocity–time curves for radial and long-axis motion indicate highly consistent global motion patters for the LV and RV (Fig. 3 top, v_r and v_z), which was confirmed by high inter-ventricular synchrony ($cc > 0.7$ for all cases). In contrast, circumferential (v_ϕ) time courses for adult and TOF patient were less synchronous ($cc = 0.53$ and $cc = -0.09$, respectively) compared to the healthy child ($cc = 0.81$). Biventricular radial peak velocities (Fig. 3 top, v_r) were similar for the three subjects ($2.3\ cm/s \leq v_{r,\ systole} \leq 4.7\ cm/s$, $-2.8\ cm/s \geq v_{r,\ diastole} \geq -4.6\ cm/s$). In contrast, long-axis diastolic peak velocities (v_z) were markedly higher in the child ($v_{z,diastole,\ LV} = -10.4\ cm/s$) compared to the adult ($v_{z,diastole,\ LV} = -3.1\ cm/s$). The TOF patient presented with a dilated RV, which was accompanied by strongly reduced systolic long-axis velocities compared to the healthy child. Slice-averaged peak velocities (Fig. 3 top, v_z) were reduced by more than 60% in systole. In diastole, regionally reduced long-axis velocities were localized at the RV free wall and the septum, resulting in markedly reduced peak velocities for both LV (by 42%) and RV (by 68%).

Table 2 Comparison of global biventricular peak velocities between two scans in ten adults

	Scan 1	Scan 2	p-value
LV			
Peak v_r (cm/s)			
Systole	3.2 ± 0.3	3.0 ± 0.3	0.3
Diastole	−3.8 ± 1.2	−3.6 ± 0.9	0.2
Peak v_z (cm/s)			
Systole	6.1 ± 2.3	6.0 ± 1.1	0.9
Diastole	−4.3 ± 2.1	−4.5 ± 1.9	0.5
Peak twist (cm/s)			
Systole	2.9 ± 0.8	2.8 ± 0.4	0.7
Diastole	−3.5 ± 1.0	−3.3 ± 1.1	0.7
RV			
Peak v_r (cm/s)			
Systole	4.5 ± 1.1	4.2 ± 0.7	0.6
Diastole	−4.1 ± 1.1	−3.9 ± 0.8	0.2
Peak v_z (cm/s)			
Systole	4.5 ± 1.6	4.3 ± 1.2	0.6
Diastole	−3.9 ± 1.4	−4.0 ± 1.2	0.5
Peak twist (cm/s)			
Systole	3.0 ± 0.9	3.4 ± 1.2	0.3
Diastole	−3.2 ± 1.3	−3.3 ± 0.9	0.8

Biventricular velocities in healthy children and adults

Findings for the individual subjects (Fig. 3) are corroborated by the cumulative results across the entire control cohort. As summarized in Table 3, global diastolic radial (v_r) peak velocities were significantly higher in children compared to adults for the LV ($p < 0.001$) and RV ($p = 0.008$). For long-axis motion (v_z), TPM detected significantly increased global peak velocities in children for LV and RV in systole ($p = 0.03$) and diastole ($p < 0.001$). Circumferential motion (v_ϕ) demonstrated significantly reduced RV diastolic peak untwist ($p < 0.05$) and increased inter-ventricular dyssynchrony (i.e. reduced cc, $p = 0.02$) for adults compared to children.

These global findings were also reflected on the segmental level as shown in Fig. 4. Regional radial and long-axis velocities during systole appeared similar between children and adults with only few segments showing significant differences (radial: reduced in 3 LV and 2 RV segments, long axis: reduced in 4 LV and 4 RV segments). In diastole, radial peak velocities were significantly lower in adults for all LV segments but in the RV only for the three inferior segments (base, mid, apex). Diastolic long-axis peak velocities were also reduced in all but one of the LV segments and six (all four basal, two mid-ventricular) RV segments.

Moreover, reduced global diastolic peak velocities were significantly associated with increased BSA for radial and long-axis components (LV v_r/v_z $r = -0.41/-0.52$, RV v_z $r = -0.44$, all $p < 0.02$, see Fig. 5).

Biventricular velocities in TOF patients

Table 3 summarizes TPM findings for TOF patients compared to age-matched healthy controls. Right ventricular long-axis (v_z) velocities were significantly reduced for TOF patients in systole and diastole ($p < 0.01$). In addition, patients showed decreased RV systolic twist compared to controls ($p = 0.001$) and increased inter-ventricular dyssynchrony (i.e. reduced cc) for radial ($p < 0.001$) and circumferential ($p = 0.02$) velocity components.

Segmental radial and long-axis peak-velocities are depicted in Fig. 6. For radial velocities, only few individual segments showed significant differences between TOF patients and controls, except for the RV in systole (reduced in five segments). Diastolic radial velocities in two LV mid-ventricular segments were significantly increased in TOF patients. Segmental long-axis velocities demonstrated more pronounced changes for both LV and RV with significantly reduced peak velocities in five LV and four RV segments in both systole and diastole. Distribution of regional LV velocities was inhomogeneous with preserved systolic and diastolic velocities in the lateral wall and significant reduction towards the septum. Segments with significantly reduced long-axis velocities were concentrated towards the base (55% of all basal compared to 35% of mid-ventricular segments) and completely absent for the apex. Velocities in the basal anterior RV segment were only available for two TOF patient and no statistical analysis could be performed for this segment.

Discussion

In this study, TPM was used to assess biventricular myocardial velocities in healthy children and adults, as well as patients with repaired TOF. The main findings of this study are: (1) TPM was feasible for the assessment of LV and RV velocities in clinically acceptable acquisition times with good test–retest reproducibility in adults. (2) TPM demonstrated similar normal LV versus RV motion patterns in both children and adults with high inter-ventricular synchrony for radial motion. (3) Comparisons of healthy adults versus children revealed significant differences in global and regional diastolic radial and long-axis peak velocities. (4) TPM detected altered biventricular long-axis velocities in TOF patients compared to age-matched controls.

Test–retest analysis for segmental biventricular peak velocities in the extended 16 + 10 AHA model confirmed

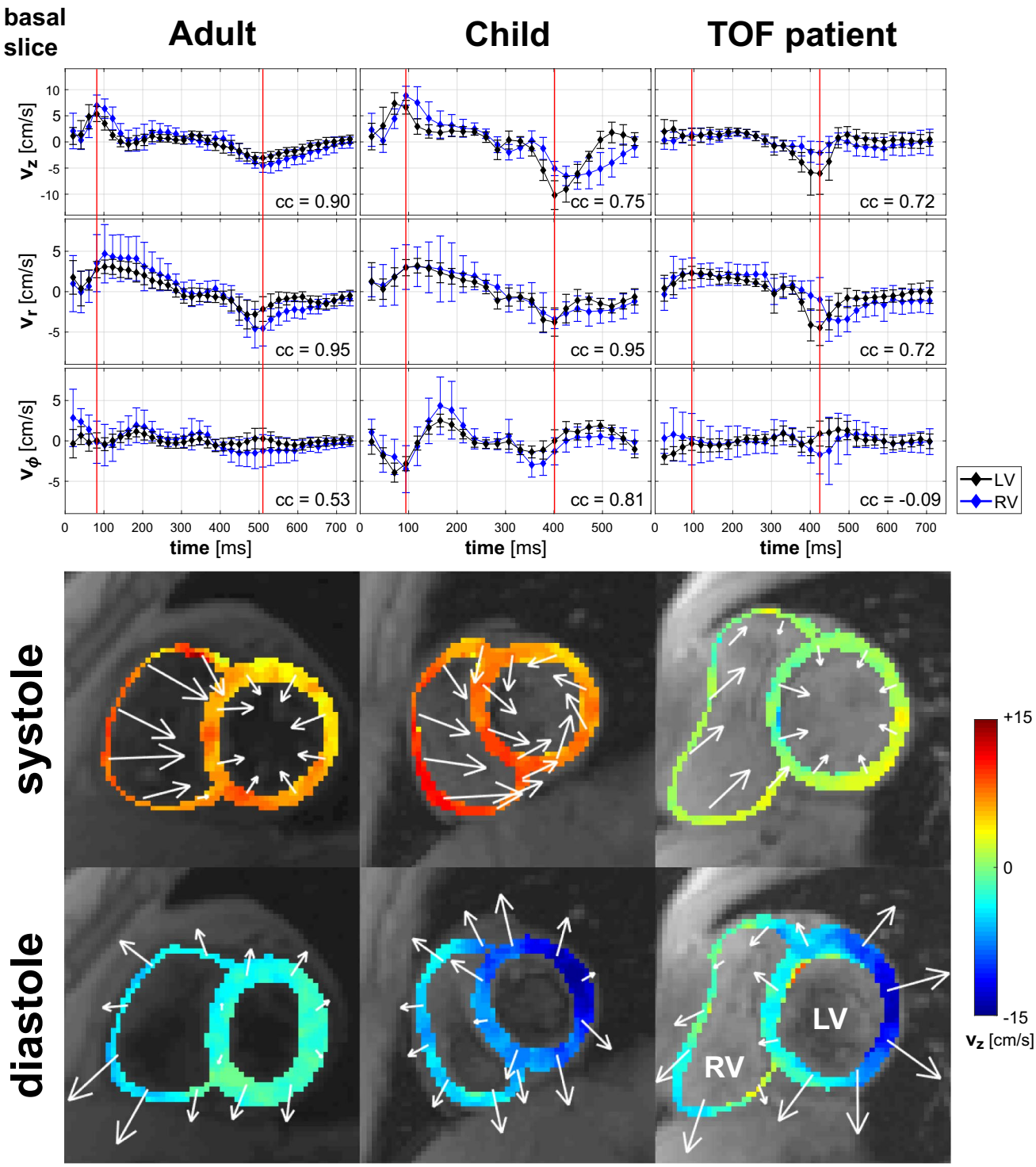

Fig. 3 Comparison of velocities in the basal slice between representative subjects (57-year-old adult, 15-year-old child, 14-year-old TOF patient). For all three components (v_z, v_r, v_ϕ), averaged velocity time courses are shown for LV (black curves) and RV (blue curves). The error bars depict the standard deviation of all velocities within the LV and RV masks. The displayed cc coefficients (here only calculated for the basal slice) quantify the synchrony/dyssynchrony between LV and RV time courses (cc = 1: completely synchronous motion, reduced cc = increased dyssynchrony). For each subject, peak systolic and peak diastolic time frames were selected (red lines) with the corresponding images shown below. Color-coded myocardial long-axis velocities were overlaid on short-axis magnitude images. In-plane velocities are depicted by regionally averaged velocity vectors

Table 3 Global biventricular peak velocities and inter-ventricular cc coefficients for healthy children and adults as well as TOF patients and age-matched controls

	Children	Adults	p-value	Controls	TOF patients	p-value
LV						
Peak v_r (cm/s)						
Systole	3.1 ± 0.5	2.9 ± 0.4	0.2	3.1 ± 0.5	3.0 ± 0.7	0.8
Diastole	**−5.1 ± 0.6**	**−3.4 ± 1.1**	**< 0.001**	−5.0 ± 0.7	−5.2 ± 1.1	0.5
Peak v_z (cm/s)						
Systole	**6.3 ± 1.7**	**5.2 ± 2.1**	**0.03**	6.2 ± 1.8	4.9 ± 1.7	0.051
Diastole	**−8.2 ± 1.4**	**−3.8 ± 1.8**	**< 0.001**	−7.9 ± 1.9	−6.5 ± 2.3	0.09
Peak twist (cm/s)						
Systole	2.5 ± 0.8	2.6 ± 0.8	0.9	2.5 ± 0.8	2.1 ± 1.1	0.3
Diastole	−3.6 ± 1.2	−3.2 ± 0.9	0.3	−3.5 ± 1.2	−3.5 ± 1.3	1.0
RV						
Peak v_r (cm/s)						
Systole	4.5 ± 1.2	4.1 ± 0.9	0.2	4.5 ± 1.2	3.5 ± 1.2	0.054
Diastole	**−4.8 ± 0.6**	**−3.9 ± 1.0**	**0.008**	−4.8 ± 0.6	−4.6 ± 1.0	0.4
Peak v_z (cm/s)						
Systole	**5.4 ± 1.6**	**4.2 ± 1.3**	**0.03**	**5.3 ± 1.6**	**3.4 ± 1.2**	**0.001**
Diastole	**−5.9 ± 1.5**	**−3.9 ± 1.3**	**< 0.001**	**−5.8 ± 1.5**	**−4.1 ± 1.5**	**0.006**
Peak twist (cm/s)						
Systole	3.6 ± 1.8	2.8 ± 1.5	0.2	**3.5 ± 1.7**	**1.5 ± 1.0**	**0.001**
Diastole	**−3.9 ± 1.3**	**−3.1 ± 1.6**	**0.048**	−3.8 ± 1.3	−2.8 ± 1.7	0.07
cc						
Radial	0.87 ± 0.03	0.83 ± 0.08	0.08	**0.88 ± 0.03**	**0.75 ± 0.09**	**< 0.001**
Long-axis	0.64 ± 0.15	0.64 ± 0.17	0.8	0.65 ± 0.14	0.66 ± 0.19	0.8
Circumferential	**0.73 ± 0.17**	**0.61 ± 0.20**	**0.02**	**0.71 ± 0.17**	**0.56 ± 0.22**	**0.02**

Bold face marks significant differences ($p < 0.05$)

cc = 1: completely synchronous LV and RV motion, reduced cc = increased dyssynchrony

the good reproducibility of TPM previously shown for the LV [35]. Similarly, an early TPM study [26] revealed good reproducibility for slice-averaged velocities, and several studies have reported low inter- and intra-observer variability [26, 29, 30, 35]. In addition, TPM reproducibility was comparable to other MR techniques assessing myocardial motion as tagging [48], feature tracking [49] or DENSE [50].

Previous TPM studies [42, 43] have analyzed biventricular cardiac function but did not quantify the synchrony between LV and RV motion. Qualitative comparisons revealed higher synchrony for radial than for long-axis or circumferential motion in healthy controls, in agreement with findings in our study (highest inter-ventricular correlation for radial velocity). Inter-ventricular dyssynchrony was previously assessed from MR tagging [10] and MR feature tracking [9, 21, 22] data using similar cross-correlation analysis to quantify time delays between LV and RV motion. However, only one of these studies analyzed more than one motion direction. In that study, similar inter-ventricular dyssynchrony was observed for circumferential and long-axis motion [9]. In general, detecting dyssynchrony is limited by the temporal resolution achieved by the imaging modality, which was about 20 ms for our TPM implementation. This is well suited to detect 50–100 ms inter-ventricular time delays reported previously for TOF patients [10, 21].

All healthy controls used in this study had normal global LV and RV function with decreased indexed volumes for adults in agreement with literature [51]. Of note, this study included children, which have been rarely studied with TPM [38, 39]. In addition, the present study is the first to investigate both LV and RV myocardial motion with TPM in children. Compared with previously studied healthy children of younger age [38, 39], LV peak velocities in this study were reduced, which agrees with the reported age dependency. Similar to our findings, prior studies demonstrated significantly decreased LV peak velocities in older subjects [28, 32]. The biventricular analysis in our study revealed that RV velocities exhibit a similar association with age (decreased RV peak velocities in adults). These findings complicate the comparison of TPM velocities with previous studies and underline the importance of age-matched control cohorts for the detection of abnormal LV and RV motion. Systolic LV peak velocities in adults are comparable to a similar age group by Föll et al. [28]. However, for diastole this study reported higher peak velocities. Considering the RV, our study found higher radial peak velocities compared

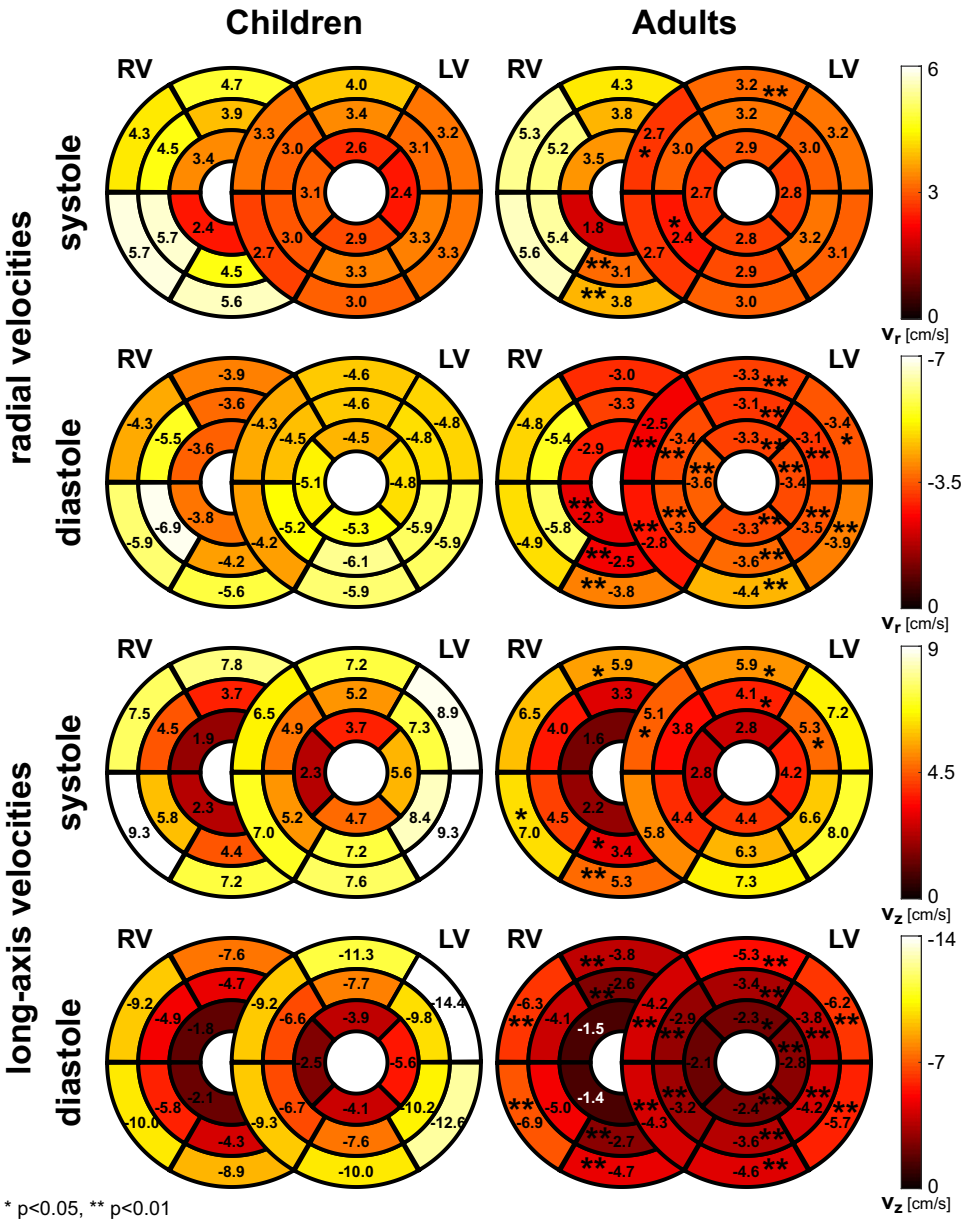

Fig. 4 Segmental radial and long-axis peak velocities in the extended 16 + 10 AHA model compared between healthy children and adults. Asterisks mark significant differences (*p < 0.05, **p < 0.01)

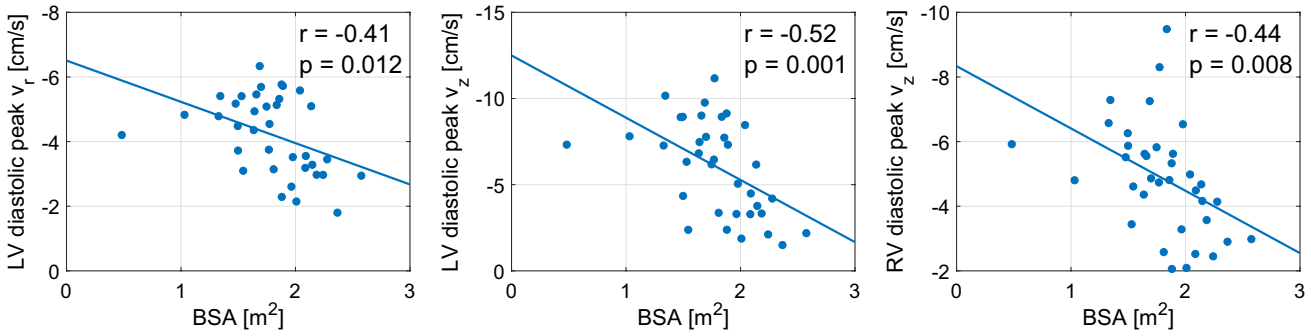

Fig. 5 Significant correlations of global diastolic radial (v_r) and long-axis (v_z) peak velocities with BSA for the combined cohort of healthy children and adults (N = 36)

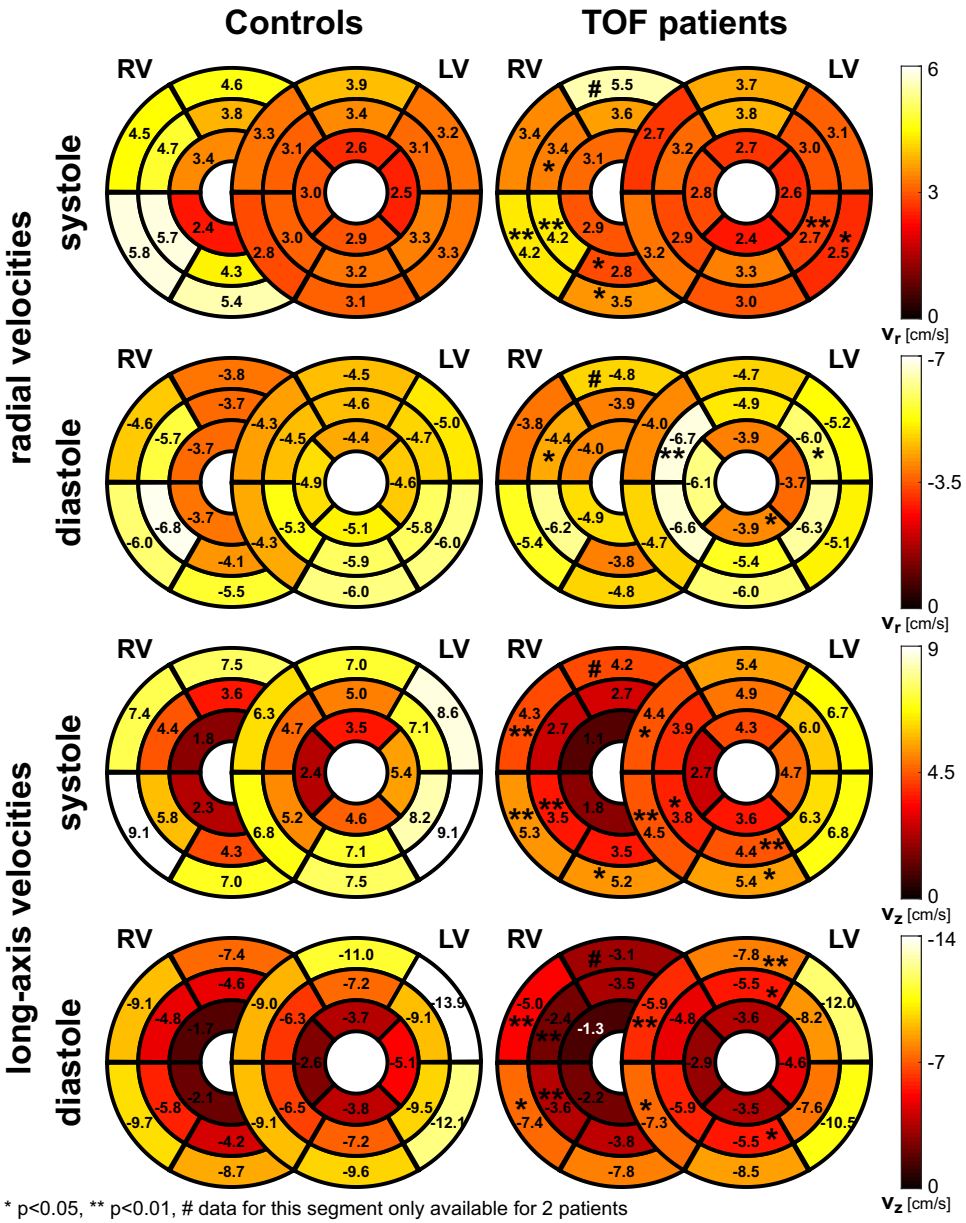

Fig. 6 Segmental radial and long-axis peak velocities in the extended 16 + 10 AHA model compared between age-matched controls and TOF patients. Asterisks mark significant differences (*p < 0.05, **p < 0.01). Due to necessary exclusions, velocities in the basal anterior RV segment (#) were only available for 2 TOF patients so that no statistical analysis could be performed for this segment

to Steeden et al. [43] but lower diastolic peak velocities than reported by Menza et al. [42]. Significant correlations with BSA suggest that also this parameter should be taken into account when analyzing myocardial velocities as it is done in echocardiography [52].

Compared to age-matched controls, TOF patients presented with impaired global biventricular function as shown by reduced LV and RV ejection fraction and increased indexed RV volumes. Impaired global function was accompanied by altered biventricular global and regional long-axis peak velocities, which were reduced by up to 50% compared to healthy controls. Since RV function plays a key role in repaired TOF [15], biventricular TPM could be an important tool for the improved characterization of this disease. However, the small patient cohort (N = 12) underlines the feasibility character of our study. In agreement with our results, a previous TPM study also found reduced LV long-axis and increased LV radial velocities in young adults with repaired TOF and preserved EF [40], which illustrates the potential of TPM to detect regionally abnormal motion before a decline in global function occurs. MR feature tracking studies reported reduced biventricular long-axis strain [8, 9]. Both MR feature tracking [21] and MR tagging [10] found increased inter-ventricular circumferential dyssynchrony in agreement with our study. In addition to MRI, also echocardiography techniques such as speckle tracking have been used to study biventricular function in pediatric TOF patients [53–55]. These studies have shown reduced

RV long-axis strain and strain rates compared to controls indicating impaired systolic and diastolic RV function in TOF patients in agreement with our results.

The present study extended previous TPM evaluations [30, 35] to the right ventricle. Regional analysis was conducted for an extended 16 + 10 AHA model as described recently [42]. To quantify biventricular interactions, a new measure for inter-ventricular dyssynchrony was introduced by calculating the cross-correlation coefficients between LV and RV velocity time courses. This analysis was conducted for all three velocity directions, whereas previous studies only investigated inter-ventricular dyssynchrony for one or two motion directions [9, 10, 21, 22]. In contrast to other biventricular TPM studies [42, 43] using free-breathing and scan times of several minutes per slice, the present TPM protocol was optimized towards clinical feasibility to acquire one slice per breath-hold.

Limitations of our study include low in-plane spatial resolution of about 2 mm to resolve the thin RV wall, which may cause partial volume effects. Improved spatial resolution could be achieved with free-breathing and navigator gating respiration control [42, 43] but would result in longer acquisition times. In our study, spatio-temporal imaging acceleration with k-t acceleration of R = 5 was utilized to achieve the most optimal spatial resolution based on the scan limitation imposed by feasible breath-hold durations. A promising alternative approach could include the combination of advanced imaging acceleration (e.g. k-t undersampling, compressed sensing) with non-Cartesian k-space acquisition [31, 37], which could further reduce the acquisition time and increase the applicability in patient groups with impaired breath-hold capabilities. Future studies are thus warranted to systematically assess the impact of spatial resolution, imaging acceleration and respiratory blurring on TPM results. Nonetheless, the good test–retest reproducibility for adult data indicates the feasibility of the TPM protocol used in the present study.

A further drawback of our study is related to the time-consuming manual segmentation of epi- and endocardium. To overcome this issue, the implementation of automatic segmentation algorithms [56, 57] into the workflow should be explored in future studies. Especially in TOF patients with their altered RV anatomy, the standardized short-axis view was often acquired at basal locations that cannot accurately capture both LV and RV myocardium. As a result, TPM data included part of pulmonary artery and/or transannular patch instead of the anterior RV wall and affected segments had to be excluded to avoid artefacts. In particular, velocity data for the anterior basal RV segment was only available for two patients, which limited the complete assessment of RV velocities. In future studies it might thus be beneficial to use adjusted short-axis or long-axis views to better capture the basal anterior RV wall. The quantification of inter-ventricular dyssynchrony in this study was based on slice-averaged velocities. However, dyssynchrony can be distributed heterogeneously within the ventricles [21, 58] and associated effects might be masked by our method. Thus, refinements towards a comprehensive dyssynchrony evaluation accounting for segmental heterogeneity should be the focus of future studies.

Another important limitation of our study is the lack of comparison to a reference standard, such as MR tagging or DENSE [59] as well as tissue doppler [60] or speckle tracking [61] echocardiography, which all require separate imaging. Alternatively, MR feature tracking [62] can be used to retrospectively assess myocardial function from standard cine images. Such comparisons should be addressed in future studies. While our study compared children with an adult group of broad age range, it would be beneficial to include additional narrower age groups as done previously for the LV [28]. Moreover, LV TPM results do not only depend on age and BSA but also show differences with gender [28]. Thus, future studies should be conducted to obtain comprehensive age and gender analysis for RV velocities. Due to the small number of TOF patients and their inhomogeneous surgical history, the presented results only indicate the feasibility of biventricular TPM. Further studies with larger cohorts including follow-up scans are needed to confirm the present results and to further investigate altered myocardial velocities in TOF patients and the diagnostic value of biventricular TPM.

In conclusion, the present study shows the feasibility of biventricular TPM for comprehensive analysis of global and regional myocardial motion and LV-RV interactions in both pediatric and adult subjects. Normal biventricular velocities were characterized by high inter-ventricular synchrony and inverse associations with age. In addition, biventricular TPM in TOF patients identified significant differences in global and regional long-axis velocities compared to age-matched controls. Larger studies are warranted to further evaluate the diagnostic value of biventricular TPM for the assessment of changes in LV and RV velocities.

Funding National Institute of Heart, Lung and Blood Disorders (NHLBI), R01 HL 117888.

Compliance with ethical standards

Conflict of interest The authors declare that they have no conflict of interest.

Ethical approval This study was approved by the institutional review boards (IRB) at Northwestern University and Ann & Robert H. Lurie Children's Hospital of Chicago.

Informed consent All adults provided written informed consent for the MRI exam. For the children, written informed consent was obtained to add the TPM sequence to a clinically indicated MRI exam.

References

1. Apostolakis S, Konstantinides S (2012) The right ventricle in health and disease: insights into physiology, pathophysiology and diagnostic management. Cardiology 121:263–273
2. Pavlicek M, Wahl A, Rutz T, de Marchi SF, Hille R, Wustmann K et al (2011) Right ventricular systolic function assessment: rank of echocardiographic methods vs. cardiac magnetic resonance imaging. Eur J Echocardiogr 12:871–880
3. Mertens LL, Friedberg MK (2010) Imaging the right ventricle—current state of the art. Nat Rev Cardiol 7:551–563
4. Galea N, Carbone I, Cannata D, Cannavale G, Conti B, Galea R et al (2013) Right ventricular cardiovascular magnetic resonance imaging: normal anatomy and spectrum of pathological findings. Insights Imaging 4:213–223
5. Fayad ZA, Ferrari VA, Kraitchman DL, Young AA, Palevsky HI, Bloomgarden DC et al (1998) Right ventricular regional function using mr tagging: normals versus chronic pulmonary hypertension. Magn Reson Med 39:116–123
6. Kayser HW, van der Geest RJ, van der Wall EE, Duchateau C, de Roos A (2000) Right Ventricular function in patients after acute myocardial infarction assessed with phase contrast MR velocity mapping encoded in three directions. J Magn Reson Imaging 11:471–475
7. Auger DA, Zhong X, Epstein FH, Spottiswoode BS (2012) Mapping right ventricular myocardial mechanics using 3D cine DENSE cardiovascular magnetic resonance. J Cardiovasc Magn Reson 14:4
8. Kempny A, Fernández-Jiménez R, Orwat S, Schuler P, Bunck AC, Maintz D et al (2012) Quantification of biventricular myocardial function using cardiac magnetic resonance feature tracking, endocardial border delineation and echocardiographic speckle tracking in patients with repaired tetralogy of fallot and healthy controls. J Cardiovasc Magn Reson 14:32
9. Moon TJ, Choueiter N, Geva T, Valente AM, Gauvreau K, Harrild DM (2015) Relation of biventricular strain and dyssynchrony in repaired tetralogy of fallot measured by cardiac magnetic resonance to death and sustained ventricular tachycardia. Am J Cardiol 115:676–680
10. Nagao M, Yamasaki Y, Yonezawa M, Matsuo Y, Kamitani T, Yamamura K et al (2015) Interventricular dyssynchrony using tagging magnetic resonance imaging predicts right ventricular dysfunction in adult congenital heart disease. Congenit Heart Dis 10:271–280
11. Hoffman JIE, Kaplan S (2002) The incidence of congenital heart disease. J Am Coll Cardiol 39:1890–1900
12. Al Habib HF, Jacobs JP, Mavroudis C, Tchervenkov CI, O'Brien SM, Mohammadi S et al (2010) Contemporary patterns of management of tetralogy of fallot: data from the society of thoracic surgeons database. Ann Thorac Surg 90:813–819
13. Helbing WA, de Roos A (2000) Clinical applications of cardiac magnetic resonance imaging after repair of tetralogy of Fallot. Pediatr Cardiol 21:70–79
14. Geva T (2011) Repaired tetralogy of Fallot: the roles of cardiovascular magnetic resonance in evaluating pathophysiology and for pulmonary valve replacement decision support. J Cardiovasc Magn Reson 13:9
15. Bonello B, Kilner PJ (2012) Review of the role of cardiovascular magnetic resonance in congenital heart disease, with a focus on right ventricle assessment. Arch Cardiovasc Dis 105:605–613
16. Valente AM, Cook S, Festa P, Ko HH, Krishnamurthy R, Taylor AM et al (2014) Multimodality Imaging Guidelines for patients with repaired tetralogy of Fallot: a report from the American Society of Echocardiography—Developed in Collaboration with the Society for Cardiovascular Magnetic Resonance and the Society for Pediatric Radiol. J Am Soc Echocardiogr 27:111–141
17. Davlouros PA, Kilner PJ, Hornung TS, Li W, Francis JM, Moon JCC et al (2002) Right ventricular function in adults with repaired tetralogy of Fallot assessed with cardiovascular magnetic resonance imaging: detrimental role of right ventricular outflow aneurysms or akinesia and adverse right-to-left ventricular interaction. J Am Coll Cardiol 40:2044–2052
18. Oosterhof T, Tulevski II, Vliegen HW, Spijkerboer AM, Mulder BJM (2006) Effects of volume and/or pressure overload secondary to congenital heart disease (tetralogy of fallot or pulmonary stenosis) on right ventricular function using cardiovascular magnetic resonance and B-type natriuretic peptide levels. Am J Cardiol 97:1051–1055
19. Yoo BW, Kim JO, Kim YJ, Choi JY, Park HK, Park YH et al (2012) Impact of pressure load caused by right ventricular outflow tract obstruction on right ventricular volume overload in patients with repaired tetralogy of Fallot. J Thorac Cardiovasc Surg 143:1299–1304
20. Khalaf A, Tani D, Tadros S, Madan S (2013) Right- and left-ventricular strain evaluation in repaired pediatric tetralogy of fallot patients using magnetic resonance tagging. Pediatr Cardiol 34:1206–1211
21. Jing L, Haggerty CM, Suever JD, Alhadad S, Prakash A, Cecchin F et al (2014) Patients with repaired tetralogy of Fallot suffer from intra-and inter-ventricular cardiac dyssynchrony: a cardiacmagnetic resonance study. Eur Heart J Cardiovasc Imaging 15:1333–1343
22. Jing L, Wehner GJ, Suever JD, Charnigo RJ, Alhadad S, Stearns E et al (2016) Left and right ventricular dyssynchrony and strains from cardiovascular magnetic resonance feature tracking do not predict deterioration of ventricular function in patients with repaired tetralogy of Fallot. J Cardiovasc Magn Reson 18:49
23. Orwat S, Diller G-P, Kempny A, Radke R, Peters B, Kühne T et al (2016) Myocardial deformation parameters predict outcome in patients with repaired tetralogy of Fallot. Heart 102:209–215
24. Hennig J, Schneider B, Peschl S, Markl M, Laubenberger TKJ (1998) Analysis of myocardial motion based on velocity measurements with a black blood prepared segmented gradient-echo sequence: methodology and applications to normal volunteers and patients. J Magn Reson Imaging 8:868–877
25. Jung B, Föll D, Böttler P, Petersen S, Hennig J, Markl M (2006) Detailed analysis of myocardial motion in volunteers and patients using high-temporal-resolution MR tissue phase mapping. J Magn Reson Imaging 24:1033–1039
26. Petersen SE, Jung BA, Wiesmann F, Selvanayagam JB, Francis JM, Hennig J et al (2006) Myocardial tissue phase mapping with cine phase-contrast MR imaging: regional wall motion analysis in healthy volunteers. Radiology 238:816–826
27. Föll D, Jung B, Staehle F, Schilli E, Bode C, Hennig J et al (2009) Visualization of multidirectional regional left ventricular dynamics by high-temporal-resolution tissue phase mapping. J Magn Reson Imaging 29:1043–1052
28. Föll D, Jung B, Schilli E, Staehle F, Geibel A, Hennig J et al (2010) Magnetic resonance tissue phase mapping of myocardial motion: new insight in age and gender. Circ Cardiovasc Imaging 3:54–64
29. Föll D, Jung B, Germann E, Staehle F, Bode C, Markl M (2013) Hypertensive heart disease: MR tissue phase mapping reveals

altered left ventricular rotation and regional myocardial long-axis velocities. Eur Radiol 23:339–347
30. Markl M, Rustogi R, Galizia M, Goyal A, Collins J, Usman A et al (2013) Myocardial T2-mapping and velocity mapping: changes in regional left ventricular structure and function after heart transplantation. Magn Reson Med 70:517–526
31. Simpson R, Keegan J, Gatehouse P, Hansen M, Firmin D (2014) Spiral tissue phase velocity mapping in a breath-hold with non-Cartesian sense. Magn Reson Med 72:659–668
32. Codreanu I, Pegg TJ, Selvanayagam JB, Robson MD, Rider OJ, Dasanu CA et al (2014) Normal values of regional and global myocardial wall motion in young and elderly individuals using navigator gated tissue phase mapping. Age 36:231–241
33. Collins J, Sommerville C, Magrath P, Spottiswoode B, Freed BH, Benzuly KH et al (2015) Extracellular volume fraction is more closely associated with altered regional left ventricular velocities than left ventricular ejection fraction in nonischemic cardiomyopathy. Circ Cardiovasc Imaging 8:e001998
34. Knight DS, Steeden JA, Moledina S, Jones A, Coghlan JG, Muthurangu V (2015) Left ventricular diastolic dysfunction in pulmonary hypertension predicts functional capacity and clinical worsening: A tissue phase mapping study. J Cardiovasc Magn Reson 17:116
35. Lin K, Chowdhary V, Benzuly KH, Yancy CW, Lomasney JW, Rigolin VH et al (2016) Reproducibility and observer variability of tissue phase mapping for the quantification of regional myocardial velocities. Int J Cardiovasc Imaging 32:1227–1234
36. von Knobelsdorff-Brenkenhoff F, Hennig P, Menza M, Dieringer MA, Föll D, Jung B et al (2016) Myocardial dysfunction in patients with aortic stenosis and hypertensive heart disease assessed by MR tissue phase mapping. J Magn Reson Imaging 44:168–177
37. Paul J, Wundrak S, Bernhardt P, Rottbauer W, Neumann H, Rasche V (2016) Self-gated tissue phase mapping using golden angle radial sparse SENSE. Magn Reson Med 75:789–800
38. Gimpel C, Jung BA, Jung S, Brado J, Schwendinger D, Burkhardt B et al (2017) Magnetic resonance tissue phase mapping demonstrates altered left ventricular diastolic function in children with chronic kidney disease. Pediatr Radiol 47:169–177
39. Brado J, Dechant MJ, Menza M, Komancsek A, Lang CN, Bugger H et al (2017) Phase-contrast magnet resonance imaging reveals regional, transmural, and base-to-apex dispersion of mechanical dysfunction in patients with long QT syndrome. Heart Rhythm 14:1388–1397
40. Chang M-C, Wu M-T, Weng K-P, Su M-Y, Menza M, Huang H-C et al (2018) Left ventricular regional myocardial motion and twist function in repaired tetralogy of Fallot evaluated by magnetic resonance tissue phase mapping. Eur Radiol 28:104–114
41. Dolan RS, Rahsepar AA, Blaisdell J, Lin K, Suwa K, Ghafourian K et al (2018) Cardiac structure-function MRI in patients after heart transplantation. J Magn Reson Imaging. https://doi.org/10.1002/jmri.26275
42. Menza M, Föll D, Hennig J, Jung B (2018) Segmental biventricular analysis of myocardial function using high temporal and spatial resolution tissue phase mapping. Magn Reson Mater Phy 31:61–73
43. Steeden JA, Knight DS, Bali S, Atkinson D, Taylor AM, Muthurangu V (2014) Self-navigated tissue phase mapping using a golden-angle spiral acquisition—proof of concept in patients with pulmonary hypertension. Magn Reson Med 71:145–155
44. Jung B, Ullmann P, Honal M, Bauer S, Hennig J, Markl M (2008) Parallel MRI With extended and averaged GRAPPA Kernels (PEAK-GRAPPA): optimized spatiotemporal dynamic imaging. J Magn Reson Imaging 28:1226–1232
45. Bauer S, Markl M, Föll D, Russe M, Stankovic Z, Jung B (2013) K–t GRAPPA accelerated phase contrast mri: improved assessment of blood flow and 3-directional myocardial motion during breath-hold. J Magn Reson Imaging 38:1054–1062
46. Cerqueira MD, Weissman NJ, Dilsizian V, Jacobs AK, Kaul S, Laskey WK et al (2002) Standardized myocardial segmentation and nomenclature for tomographic imaging of the heart: a statement for healthcare professionals from the Cardiac Imaging Committee of the Council on Clinical Cardiology of the American Heart Association. Circulation 105:539–542
47. Walker PG, Cranney GB, Scheidegger MB, Waseleski G, Pohost GM, Yoganathan AP (1993) Semiautomated method for noise reduction and background phase error correction in MR phase velocity data. J Magn Reson Imaging 3:521–530
48. Donekal S, Ambale-Venkatesh B, Berkowitz S, Wu CO, Choi EY, Fernandes V et al (2013) Inter-study reproducibility of cardiovascular magnetic resonance tagging. J Cardiovasc Magn Reson 15:37
49. Maceira AM, Tuset-Sanchis L, López-Garrido M, San Andres M, López-Lereu MP, Monmeneu JV et al (2018) Feasibility and reproducibility of feature-tracking-based strain and strain rate measures of the left ventricle in different diseases and genders. J Magn Reson Imaging 47:1415–1425
50. Lin K, Meng L, Collins JD, Chowdhary V, Markl M, Carr JC (2017) Reproducibility of cine displacement encoding with stimulated echoes (DENSE) in human subjects. Magn Reson Imaging 35:148–153
51. Kawel-Boehm N, Maceira A, Valsangiacomo-Buechel ER, Vogel-Claussen J, Turkbey EB, Williams R et al (2015) Normal values for cardiovascular magnetic resonance in adults and children. J Cardiovasc Magn Reson 17:29
52. Dallaire F, Slorach C, Hui W, Sarkola T, Friedberg MK, Bradley TJ et al (2015) Reference values for pulse wave Doppler and tissue Doppler imaging in pediatric echocardiography. Circ Cardiovasc Imaging 8:e002167
53. Friedberg MK, Fernandes FP, Roche SL, Grosse-Wortmann L, Manlhiot C, Fackoury C et al (2012) Impaired right and left ventricular diastolic myocardial mechanics and filling in asymptomatic children and adolescents after repair of tetralogy of Fallot. Eur Heart J Cardiovasc Imaging 13:905–913
54. Friedberg MK, Fernandes FP, Roche SL, Slorach C, Grosse-Wortmann L, Manlhiot C et al (2013) Relation of right ventricular mechanics to exercise tolerance in children after tetralogy of Fallot repair. Am Heart J 165:551–557
55. Dragulescu A, Friedberg MK, Grosse-Wortmann L, Redington A, Mertens L (2014) Effect of chronic right ventricular volume overload on ventricular interaction in patients after tetralogy of Fallot repair. J Am Soc Echocardiogr 27:896–902
56. Chitiboi T, Hennemuth A, Schnell S, Chowdhary V, Honarmand A, Markl M et al (2016) Contour tracking and probabilistic segmentation of tissue phase mapping MRI. Proc SPIE 9784:978404
57. Espe EKS, Skårdal K, Aronsen JM, Zhang L, Sjaastad I (2017) A semiautomatic method for rapid segmentation of velocity-encoded myocardial magnetic resonance imaging data. Magn Reson Med 78:1199–1207
58. Suever JD, Fornwalt BK, Neuman LR, Delfino JG, Lloyd MS, Oshinski JN (2014) Method to create regional mechanical dyssynchrony maps from short-axis cine steady-state free-precession images. J Magn Reson Imaging 39:958–965
59. Simpson RM, Keegan J, Firmin DN (2013) MR assessment of regional myocardial mechanics. J Magn Reson Imaging 37:576–599
60. Jung B, Schneider B, Markl M, Saurbier B, Geibel A, Hennig J (2004) Measurement of left ventricular velocities: phase contrast MRI velocity mapping versus tissue-Doppler-ultrasound in healthy volunteers. J Cardiovasc Magn Reson 6:777–783
61. Geyer H, Caracciolo G, Abe H, Wilansky S, Carerj S, Gentile F et al (2010) Assessment of myocardial mechanics using speckle

tracking echocardiography: fundamentals and clinical applications. J Am Soc Echocardiogr 23:351–369
62. Schuster A, Hor KN, Kowallick JT, Beerbaum P, Kutty S (2016) Cardiovascular magnetic resonance myocardial feature tracking: concepts and clinical applications. Circ Cardiovasc Imaging 9:e004077